1   **Late Quaternary sea level changes of the Persian Gulf**

2

3   Stephen W. Lokier [a,*], Mark D. Bateman [b], Nigel R. Larkin [c], Philip Rye [d] and John R. Stewart [e]

4

5   [a] Petroleum Geosciences Department, The Petroleum Institute, P.O. Box 2533, Abu Dhabi, United

6   Arab Emirates (slokier@pi.ac.ae)

7   [b] Department of Geography, Winter St., University of Sheffield, Sheffield, S10 2TN, UK

8   (M.D.Bateman@sheffield.ac.uk)

9   [c] Cambridge University Museum of Zoology, Downing Street, Cambridge, CB2 3EJ, UK

10   (nrlarkin@easynet.co.uk)

11   [d] Granary Court Cottage, Granary Court Road, Smeeth, Ashford, Kent, TN25 6RE, UK

12   (phil_rye@hotmail.com)

13   [e] School of Science and Technology, Bournemouth University Talbot Campus, Fern Barrow Poole,

14   Dorset, BH12 5BB, UK (jstewart@bournemouth.ac.uk)

15   [*] Corresponding author.

16   E-mail address: slokier@pi.ac.ae (S. Lokier)

17

18   **Abstract**

19   Late Quaternary reflooding of the Persian Gulf climaxed with the mid-Holocene highstand previously

20   variously dated between 6 – 3.4 ka. Examination of the stratigraphic and palaeoenvironmental

21   context of a mid-Holocene whale beaching allows us to accurately constrain the timing of the

22   transgressive, highstand and regressive phases of the mid- to late Holocene sea level highstand in

23   the Persian Gulf. Mid-Holocene transgression of the Gulf surpassed today's sea level by 7100-6890

24   cal yr BP, attaining a highstand of > 1 m above current seal level shortly after 5290-4570 cal yr BP

25   before falling back to current levels by 1440-1170 cal yr BP. The cetacean beached into an intertidal

26   hardground pond during the transgressive phase (5300-4960 cal yr BP) with continued transgression

27   interring the skeleton in shallow-subtidal sediments. Subsequent relative sea level fall produced a

28   forced regression with consequent progradation of the coastal system. These new dates refine

29   previously reported timings for the mid- to late Holocene sea level highstand published for other

30   regions. By so doing, they allow us to more accurately constrain the timing of this correlatable global

31   eustatic event.

32   *Keywords***:** Persian Gulf; Arabian Gulf; Sabkha; Sea level; OSL; Quaternary

33

34   **Introduction**

35   The present-day morphology of the Abu Dhabi coastline of the United Arab Emirates is interpreted

36   to have developed during the late Holocene as sediment accreted around Pleistocene age limestone

37   cores, associated with the eastern termination of the Great Pearl Bank, and prograded into the

38   recently-flooded Persian Gulf (e.g. Evans et al., 1969; Lokier and Steuber, 2008; Purser and Evans,

39   1973). However, establishing the timing of the Holocene sea level maximum for the Persian Gulf,

40   and, hence, the initiation of late Holocene progradation of the Abu Dhabi shoreline, has been

41   problematical. This study employs sedimentary sections hosting a cetacean skeleton as a data source

42   to provide new evidence for the constraint of the Holocene sea level maximum in the Persian Gulf.

43   During the Last Glacial Maximum (LGM), between 26.5 and 19 ka (Clark et al., 2009), eustatic sea

44   level lay between 120 – 130 m lower than present-day sea level (Clark et al., 2009; Fleming et al.,

45   1998; Hanebuth et al., 2009; Peltier and Fairbanks, 2006). During this time, the sea floor of the

46   Persian Gulf was exposed and terrestrial aeolian processes became dominant. The northwesterly

47   Shamal wind blew sand, sourced from Iran, towards the south and east and an extensive dune

48   system developed over much of the basin floor (Sarnthein, 1972). With the end of the LGM, between

49   20-19 ka (Clark et al., 2009; Yokoyama et al., 2000), a pulse of fresh water caused a rapid sea level

50   rise of 10 m (Clark et al., 2009; Hanebuth et al., 2009), followed by a slower, relatively sedate,

51   increase. Marine waters reached the Strait of Hormuz at approximately 14 ka and by 12.5 ka had

52   entered the Gulf itself and a true seaway had been established (Lambeck, 1996).

53   The objectives of this study are to utilise a whale beaching event to refine the timing and amplitude

54   of the Holocene sea level maximum in the Persian Gulf and establish the palaeoenvironmental and

55   sequence stratigraphic context of the coastal system at that time. By understanding these factors it

56   will be possible to establish better-constrained sedimentological and stratigraphic models for the

57   development of the Holocene sabkhas of the southern shoreline of the Persian Gulf. These systems

58   are the oft-cited analogue for many of the petroleum reservoirs of the Middle East, thus, an

59   understanding of their mode of formation is imperative to the interpretation of ancient petroleum

60   systems and the development of accurate reservoir models.

61

62   *Location of study area*

63   The study site lies in the Mussafah Channel situated in the Mussafah Industrial Zone of Abu Dhabi

64   (Fig. 1). The Mussafah Channel is an 8.3 km long dredged channel that was excavated through the

65   coastal Sabkha sequence during the early 1980's. As no further development of the channel took

66   place, the unsupported walls collapsed and eroded back to expose fresh surfaces. Erosion continued

67   until 2006 when a cetacean mandible was exposed at the eastern termination of the channel.

68   Excavation revealed a largely-intact skeleton of a baleen whale of the genus *Megaptera* (Stewart et

69   al., 2011) of which the front 10 m was recovered, including the most-diagnostic cranial and forelimb

70   parts.

71   *Geographic and climatic setting*

72   The Persian Gulf is a shallow epicontinental sea lying in a crescentic northwest to southeast oriented

73   basin floored by the continental crust of the northern margin of the Arabian Plate (Fig. 1). The Zagros

74   Mountains bound the northern shores while the south and west shorelines are bordered by the low-

75   relief Arabian Peninsula. Water depths are shallow, with an average depth of 35 m and rarely exceed

76   100 m. The floor of the Gulf dips gently north-eastward with the deepest water areas lying close to

77   the southern coast of Iran.

78   The Persian Gulf coastline of the emirate of Abu Dhabi forms part of a low-angle carbonate ramp

79   depositional system. The supratidal zone of this ramp is characterised by an active sabkha setting in

80   which Recent evaporite minerals are precipitating within the shallow subsurface and an ephemeral

81   halite crust at the surface (Lokier, 2012). The sabkha grades seawards into a broad intertidal mud

82   flat with well-developed microbial mat communities characterising the upper intertidal zone and a

83   polygonal hardground in the lower intertidal zone (Lokier and Steuber, 2009). The hardground

84   extends offshore into the shallow, carbonate-dominated subtidal setting. The mainland coast of Abu

85   Dhabi is locally protected from open-marine conditions by a number of peninsulas and offshore

86   shoals and islands (Fig. 1) associated with the east–west trending Great Pearl Bank. The limited fetch

87   of the Persian Gulf inhibits wave development, thus, low-energy conditions dominate. The tidal

88   regime of the Persian Gulf is microtidal (1–2 m).

89   The very low-angle geometry of the Abu Dhabi coastline results in this region being extremely

90   sensitive to fluctuations in sea level. Even small changes in relative sea level will result in significant

91   lateral shifts in facies belts. For example, current estimates of eustatic sea level rise of 3.3 mm/yr

92   (Cazenave and Nerem, 2004; Leuliette et al., 2004) would result in marine transgression of the Abu

93   Dhabi shoreline at a rate of 8.25 m/yr. This transgression is, to some extent, countered by

94   progradation of the sabkha system (Lokier and Steuber, 2008). The sensitivity of this coastal system

95   to minor sea level fluctuations provides an opportunity to apply these findings beyond the

96   immediate region of the Persian Gulf to further constrain the timing and extent of the mid- to late

97   Holocene global sea level highstand.

98   The climate at the Abu Dhabi coast is extremely arid with a mean annual precipitation of 72 mm

99   (Raafat, 2007). Rainfall is often extremely localised, occurring as brief heavy rainstorms concentrated

100   during the months of February and March. Some regions may not experience any rainfall for periods

101   in excess of a year. Evaporation rates are high with an annual mean of 2.75 m (Bottomley, 1996)

102   resulting in elevated salinities of 45–46 g l^{-1} along the open-marine coast of Abu Dhabi and up to 89

103   g l^{-1} in restricted lagoons (Lokier and Steuber, 2009). Coastline temperatures 50 km west of Abu

104   Dhabi City range between 7°C at night during the winter and 50°C during daytime in the summer

105   (Lokier et al., 2013). The prevailing wind is the north-westerly Shamal. The shallow warm waters of

106   the coast generate high coastal humidity, often reaching 100% during summer months.

107

108   **Methodology**

109   The site was surveyed utilising a Leica total station employing the Admiralty Chart Datum of mean

110   lowest calculated astronomical tide. The stratigraphy of the sediments was recorded in detail at

111   three locations, facies geometries were characterised and representative sediment samples were

112   collected throughout the profile. Unconsolidated sediment samples were prepared as twenty four

113   resin-impregnated thin sections. Thin sections were subjected to modal analysis, 200 points, in order

114   to quantify the proportions of component allochems. In order to further characterise sedimentary

115   facies, thin sections were examined using standard light microscopy on a polarising microscope.

116   Sediment and skeletal allochem samples were also collected from throughout the excavation site

117   with particular attention being given to their relationship to the cetacean bones.

118   Five samples were designated for radiocarbon analysis via accelerator mass spectrometry (AMS) at

119   the [14]Chrono Centre, Queens University, Belfast. During sample selection, skeletal material from

120   deposit-feeding organisms was avoided as these organisms may ingest detrital ancient carbon which

121   will become incorporated into their shells and significantly offset ^{14}C ages. All of the selected

122   samples were subjected to detailed examination in order to protect against taphonomic processes

123   that would bias radiocarbon analysis. The selected material comprised three bivalves, one barnacle

124   and one specimen of cetacean bone. Unfortunately, the initial elemental analysis of the sample of

125   whale bone (MUS 17B) indicated that there was insufficient remaining protein to undertake

126   radiocarbon dating. All of the ^{14}C results are presented as conventional radiocarbon ages employing

127   the Libby half-life method (Stuiver and Polach, 1977). Results were calibrated using the CALIB

128   (version 7.0.0) calibration program (Stuiver and Reimer, 1993) employing a marine calibration curve

129   and a regional reservoir age correction (ΔR) of 180 ± 53 (Hughen et al., 2004).

130   Optically stimulated luminescence (OSL) dating was undertaken on three samples collected from

131   sediment found directly adjacent to the whale skeleton. Samples were analysed at the Luminescence

132   Dating Laboratory of the Sheffield Centre for Drylands Research (SCIDR). The palaeodose of quartz

133   grains was measured on 9.6 mm diameter aliquots by employing a modified form of the single

134   aliquot regenerative (SAR) method (Murray and Wintle, 2000) using a Risø TL DA-20 luminesce

135   reader with radiation doses administered from a calibrated [90]strontium beta source. An

136   experimentally derived preheat of 180°C for 10 seconds and a cut-heat of 160°C was used within the

137   SAR. During testing with infrared stimulated luminescence (IRSL) it was found that a residual feldspar

138   signal existed within the samples (possibly due to feldspars included within quartz), which was

139   removed prior to each OSL SAR measurement with an IRSL wash for 40 seconds at 50°C (Banerjee et

140   al., 2001; Wilson et al., 2008). Reproducibility was established by undertaking up to 24 replicate

141   palaeodoses on each sample. The above methodology was validated with a dose recovery test on

142   sample Shfd11039 which returned a given to recovered dose ratio of 0.97 ± 0.02. Final palaeodoses

143   for each samples were derived from this replicate data using the central age model (Galbraith and

144   Green, 1990) excluding outliers (those aliquots outside 2 standard deviations of the mean).

145   Elemental concentrations were determined from ICP-MS analysis with the resultant uranium,

146   thorium, rubidium and potassium values being used, once suitably attenuated for moisture (a

147   saturation value of 30 ± 5% was applied), size and density to calculate sample dose rates.

148   Cosmogenic contributions were calculated using the algorithm of Prescott and Hutton (1994).

149   Samples for the analysis of δ^{18}O and δ^{13}C were prepared from three thick sections of articulated

150   filter-feeding bivalves. Powder was milled from the thick sections parallel to growth bands using a

151   0.8 mm diameter tungsten drill bit. Samples were analysed at GeoZentrum Nordbayern using a

152   Gasbench II connected to a ThermoFinnigan Five Plus mass spectrometer. External reproducibility is

153   better than 0.1‰ δ^{18}O and δ^{13}C at 2 sigma.

154

155   **Results**

156   *Stratigraphic context of the cetacean skeleton*

157 Three stratigraphic sections were logged in detail for this study (Fig. 2). The sections all lie on a

158 north-south transect along the eastern wall of the Mussafah Channel, and were selected in order to

159 avoid areas with any evidence of anthropogenic disturbance. The central section (MC-3) lies within

160 the excavation site and records the relationship between sedimentary facies and the skeleton (Figs 3

161 & 4).

162 The base of the stratigraphic succession is only observed in section MC-1 where it comprises a grey

163 peloidal and bioclastic carbonate sand with large gypsum lathes up to 30 cm in diameter (Table 1,

164 Figs 2 & 5). This horizon is overlain by a locally-degraded laminated microbial mat containing isolated

165 bioclasts bound within the laminations. The microbial mat horizon is overlain by a carbonate-

166 cemented planar hardground dominated by bioclasts but with isolated gypsum lathes. The planar

167 surface of the hardground lacks any evidence of encrustation or boring. Above the hardground,

168 locally-laminated peloidal bioclastic carbonate sand becomes increasingly mud-dominated up-

169 section (Table 1) before passing into a horizon of bioturbated, poorly-laminated muddy facies that

170 again contains peloids and bioclasts. This horizon is locally bioturbated by mm-wide sub-vertical

171 burrows with distinctive dark-brown margins. Locally cross-bedded bioclastic gravels, dominated by

172 gastropods, bivalves and peneroplid foraminifera, are banked against some of the bones of the

173 skeleton, these gravel banks do not exhibit any preferred orientation. The succeeding unit is a peloid

174 and bioclastic sand with mud. The top of the succession comprises gypsum gravel with an increasing

175 anhydrite component in the uppermost portion (Table 1). The anhydrite is locally distorted to form

176 an enterolithic texture (Figs 2 & 4B). Gypsum lathes occur throughout the succession with a decrease

177 in size up-section. Siliciclastic material was only observed in the hardground and underlying units

178 (Fig. 5). A series of iron-oxide stained horizons occur at a depth of 26-53 cm below the surface of the

179 sediment; these stains form bands between 1-4 cm in thickness with the most-stained and thickest

180 band occurring at their base (Figs 2 & 4B).

181   The skeleton of the cetacean lies, in an inverted position, atop the hardground within the peloidal

182   bioclastic carbonate sand and mud horizons. The lower portions of the jaws and skull locally

183   penetrate into, and are embedded within, the underlying hardground. Locally, articulated bivalves

184   (*Saccostrea*) were found attached to the ribs close to the vertebrae. The sediments adjacent to the

185   skeleton exhibit lateral variability both in terms of grain size and component allochems (Table 1).

186

Dating the stratigraphic sequence

188   The calculated radiocarbon dates are presented in Table 2 along with the calibrated age ranges and

189   delta ^{13}C values for the samples. The reported δ^{13}C values are appropriate for the nature of the

190   materials being considered in the study (Walker, 2005). The calibrated ages are internally consistent

191   with the oldest date (6887-6567 cal yr BP) being recorded from the hardground, an age of 5304-

192   4957 cal yr BP being recorded for a barnacle identified as *Coronula diadema* that is believed to have

193   been attached to the whale's skin in life (Stewart et al., 2011) and so dates the whale at death and

194   the youngest ages (5285-4574 cal yr BP) being recorded from the sediments surrounding the

195   skeleton. These dates are consistent with previously published radiocarbon dates for the upper part

196   of the Mussafah Channel sedimentary sequence (Stewart et al., 2011; Strohmenger et al., 2010).

197   Previously reported ages for the microbial mat range between 6230-7103 cal yr BP (Stewart et al.,

198   2011) but must predate the hardground that has been dated at 6887-6567 cal yr BP. Thus, we can

199   constrain the age of the microbial mat to between 7103-6887 cal yr BP.

200   The results of the OSL analysis are presented in Table 3 along with palaeodose and calculated dose

201   rates for the samples. The derived ages, of between 3.18 ± 0.24 – 2.51 ka ± 0.14, are also internally

202   consistent but are significantly younger than those calculated for the equivalent horizons using

203   radiocarbon analysis. These large discrepancies between the radiocarbon dates and the dates

204   derived from OSL are a cause for concern. As stated, the radiocarbon dates are consistent with ages

205 published from earlier studies of the Abu Dhabi Sabkha sequence, it is therefore inferred that the

206 OSL dates are problematical.

207 The OSL replicate palaeodose data is essentially normally distributed, showing little scatter apart

208 from an occasional outlier (2, 4 and 5 aliquots from Shfd11039-42 respectively) and a dose can be

209 recovered successfully in the lab. It would appear unlikely that the OSL ages are too young as a result

210 of mixing in of younger sediment due to bioturbation (Bateman et al., 2007) or incorrect

211 measurement.

212 OSL relies on establishing the average burial environmental dose rate in order to calculate the age of

213 the sample. Environmental dose rate is controlled by the presence of radioactive elements (uranium

214 (U), thorium (Th) , rubidium (Rb), potassium-40 (K)) and cosmic rays. The presence of water is also

215 important as it absorbs radiation differently from the sediment (Lian et al., 1995). During OSL date

216 calculation, it was assumed that the average moisture since burial was at saturation (30%). This

217 assumption is based on the presence of the iron-stained horizons which show that, prior to the

218 excavation of the Mussafah Channel, the site lay wholly below the water table. This then is not the

219 source of OSL age under-estimation.

220 Both uranium and potassium are soluble, therefore it is possible that fluctuating saline groundwater,

221 coupled with a high evaporation rate, could have modified the environmental radiation dose since

222 burial by leaching and concentrating these elements. Whilst it is not possible to reconstruct changes

223 of dose rate through time, two observations can be made. Firstly, both U and K increase with depth

224 and secondly the Th:U ratio for the three samples is 0.22, this is significantly different than the upper

225 continental crustal average (UCC) of 3.82 (Taylor and McClennan, 1985). It is therefore possible that

226 the elemental concentrations, as measured, do not reflect the average concentrations during the

227 burial history of the sediments. Similar disequilibrium issues were identified in Wood et al. (2012)

228 and Stevens et al. (2014) from Persian coastal samples. In these studies, conservative (large)

229   uncertainties were applied to correct ages for disequilibrium. In the current study we can show with

230   the benefit of the independent radiocarbon chronology that this approach doesn't work for young

231   samples. If, however, an average UCC is applied to the data by reducing the U concentrations (i.e.

232   assuming present-day values reflect recent concentration) OSL ages are brought into line with those

233   of radiocarbon (5.31 ±0.27 to 6.76 ±0.34 ka; Table 3). The true validity of the corrected age estimates

234   is open to question but is illustrative of the probable cause of the age disagreement with the

235   radiocarbon data. As a result of the uncertainties surrounding the OSL chronology this has been

236   excluded from subsequent interpretation and discussion.

237

238   *Palaeotemperature*

239   Mean annual palaeotemperatures were calculated following Goodwin et al. (2003) using the

240   equation: temperature = 20.6 – 4.34 [$\delta^{18}O_{aragonite}$ – ($\delta^{18}O_{water}$ - 0.2)] (Table 4). A value of +3 ‰ was

241   applied for $\delta^{18}O_{water}$ in accordance with the relationships observed from the analysis of Recent

242   marine water samples taken from offshore Abu Dhabi (Lokier and Steuber, 2009). The two *Pinctada*

243   specimens yielded palaeotemperatures of 27.7°C and 30.5°C while the *Barbatia* specimen yielded a

244   palaeotemperature of 22.6°C (Table 4). The differences in these results are reconcilable as *Pinctada*

245   are often associated with mid to lower shore settings while *Barbatia* is associated with deeper,

246   lower shore to sublittoral, environments (Bosch et al., 1995). These temperatures are entirely

247   consistent with the temperatures observed along the coastline of Abu Dhabi today with surface

248   temperatures ranging between 22-37°C (Evans et al., 1973) while temperatures below 4-5 m water

249   depth range between 20-36°C (Kinsman, 1964).

250

251   **Interpretation and discussion**

Palaeoenvironmental context of the skeleton

The siliciclastic material within the lowermost units of the sedimentary sequence is inferred to have been derived from the underlying quartz-rich sands as documented by Kirkham (1998). These sands have previously been interpreted as being deposited as aeolian dunes and are dated from prior to the post-glacial reflooding of the Persian Gulf (Evans et al., 1969) with ages between 26,760 (±180) ^{14}C yrs BP and 24,010 (±150) ^{14}C yrs BP proposed by Strohmenger et al. (2010). However, as these dates are derived from bulk samples of sediment, they should be treated with a degree of caution as there is a strong likelihood of the samples being contaminated with carbonate material from a wide range of sources and with a wide range of ages. During transgression these aeolian sands were locally eroded and admixed into the overlying transgressive quartz-rich carbonate unit.

The overlying microbial mat (Fig. 2) has previously been interpreted as a transgressive unit (Kenig et al., 1990). Recent microbial mat communities are well-developed in the Recent Abu Dhabi sabkha where they form a belt marking the landward-limit of the intertidal zone (Lokier and Steuber, 2008). At this position, brief periods of flooding prevent complete desiccation of the mats whilst regular exposure inhibits predation by grazing marine gastropods. The microbial mat horizon observed in the Mussafah Channel section is here inferred to record a similar stressed upper intertidal environment. Its stratigraphic position, immediately overlying the transgressive quartz-rich carbonate sands, is consistent with a slowing in transgression or a stillstand.

In the Recent Abu Dhabi sabkha the microbial mats are typically only 1-5 cm in thickness. The development of thicker microbial mats is limited to depressions in the upper intertidal zone where water is able to pond following spring high tides. Evaporation from these ponds results in elevated salinities that prohibit colonisation by grazing fauna, thereby allowing successive generations of microbial mat to build laminated units until the ponds are infilled. The microbial mat observed in the Mussafah Channel section is 11 cm in thickness (Fig. 2). This may be attributed to the flooding of

276 antecedent dune topography followed by a stillstand. Subtle variations in relief would result in local

277 variations in water depth with isolated shallow basins permitting the development of locally thicker

278 microbial mat units.

279 The hardground that immediately overlies the microbial mats (Fig. 2) is interpreted to have

280 developed in the lower intertidal to subtidal zone, a setting in which hardgrounds are developing in

281 the Persian Gulf today (Lokier and Steuber, 2009; Shinn, 1969). This implies renewed transgression

282 following deposition of the microbial mat horizon (Fig. 6). The preservation of the underlying

283 microbial mats during transgression is problematic since marine flooding will place the mats in an

284 environment where gastropods or other marine organisms are able to actively graze upon them.

285 However, if transgression was rapid, then it is feasible that the microbial mats would be promptly

286 buried, thus preserving them from grazing epifauna. Buried mats would remain vulnerable to

287 destruction through the activities of burrowing deposit-feeding organisms. However, the modern

288 microbial mats are observed to be anoxic at shallow depths below the surface. Such anoxia would

289 inhibit infaunal activity. The development of hardgrounds can be rapid, crusts may form in less than

290 20 years (Shinn, 1969), thus aiding the preservation of underlying microbial mats.

291 Recent intertidal hardgrounds form large-scale (>100 m diameter) polygons with a dish-like

292 morphology comprising a planar interior and gently-uplifted margins. The polygons retain water to

293 form shallow (10 cm) ponds at low tide and are totally inundated, and recharged, during high tides.

294 The interior of these intertidal polygons is covered by a thin (3-5 cm) veneer of sediment that may

295 be temporarily removed during high-energy storm events (Lokier and Steuber, 2009). Beneath this

296 veneer is a poorly-lithified firmground of 1-4 cm thickness that represents the zone of active

297 cementation (Lokier and Steuber, 2009). Beneath the firmground is the hardground proper. The

298 presence of the unlithified sediment veneer prohibits encrustation by benthic communities over

299 most of the hardground surface; encrustation is limited to the exposed uplifted polygon margins

300 where a diverse range of benthos is observed.

301   The lower portions of the cetacean jaws and skull are locally embedded within the hardground; the

302   cetacean must therefore have been emplaced into the intertidal zone prior to the completion of

303   lithification. As the bones do not completely penetrate through the hardground, it is likely that the

304   hardground had already begun to lithify prior to the arrival of the cetacean. Following arrival, the

305   heavier bones of the jaw and skull would have penetrated into the firmground to become cemented

306   during continued hardground development. The presence of encrusting benthos on the low-lying

307   bones proves that the lower portion of these bones must have been regularly submerged and

308   supports the interpretation of emplacement of the cetacean onto a shallow, lower intertidal

309   hardground pond. The interpretation of emplacement of the whale into a shallow intertidal

310   hardground pond is supported by the low-diversity of the ostracod assemblage as previously

311   documented from the Mussafah Channel (Stewart et al., 2011) as these ponds are known to have

312   high salinities today.

313   Previous studies have hypothesised that the cetacean was emplaced into a tidal channel (Stewart et

314   al., 2011; Strohmenger et al., 2010). However, we do not support this interpretation for the

315   following reasons: 1) Tidal channels typically concentrate water flow during the ebb tide; therefore

316   they are a focus of off-shore transport. As such, it is unlikely that, once emplaced, a carcass would

317   remain for very long in such a setting. 2) Tidal channels are high-energy features, typically with

318   erosive bases. There is no evidence of an erosive base at the whale excavation site. 3) The high

319   energies that are typical of tidal channels would rapidly disarticulate the skeleton and transport the

320   smaller bones, such as the phalanges, offshore. 4) The presence of coarse-grained bioclastic material

321   banked against the bones is unlikely to occur in a tidal channel where such material is easily

322   transported off-shore. 5) Any hard substrates in channels are heavily encrusted by marine benthos

323   yet only the lowermost portions of the skeleton were encrusted.

324   The remarkably planar surface of the hardground in the Mussafah Channel (Fig. 4) has previously

325   been interpreted as a possible aeolian erosional feature in which the surface of the hardground was

326   wind-planed (Kirkham, 1998). However, as some of the cetacean bones clearly penetrate, and are

327   cemented within, the hardground this interpretation is deemed to be unlikely, as such an intense

328   process would have caused significant abrasion and, weathering of the skeleton.

329   The excellent state of preservation and relatively complete articulation of the bones is consistent

330   with relatively rapid burial following emplacement. The stratigraphic sequence overlying the

331   hardground, and containing the cetacean skeleton, exhibits an overall fining-upward trend (Figs 2

332   and 5) that implies a reduction in energy regimes consistent with deepening of the

333   palaeoenvironment during continued transgression. This subtidal sequence differs significantly from

334   the progradational sedimentary sequence described previously from elsewhere in the Abu Dhabi

335   sabkha (Evans et al., 1969; Kirkham, 1998; Lokier and Steuber, 2008). Of particular interest is the lack

336   of a microbial mat horizon at the contact between the carbonate-dominated intertidal sediments

337   and the overlying supratidal evaporite-dominated units in the Mussafah Channel section. As

338   mentioned previously, microbial mats demark the uppermost intertidal zone and, during

339   progradation, are likely to be preserved, even following shallow burial, on entering the supratidal

340   environment. Their absence from the Mussafah Channel section is consistent with a rapid fall in sea

341   level resulting in rapid progradation of the shoreline without allowing sufficient time for significant

342   microbial mat development. The succeeding, laterally discontinuous, peloidal and skeletal muddy

343   sand horizons are inferred to represent the abandonment of storm-surge emplaced beach ridges

344   during this regression. The uppermost unit in the sequence records the displacive growth of gypsum,

345   and near-surface anhydrite, in a supratidal sabkha setting.

346   The bioclast-rich sandy gravels banked against the bones are inferred to have been transported and

347   deposited during storm surges. The accumulation of coarse-grained sediments against obstructions

348   is a common feature in the intertidal zone of the Recent sabkha of Abu Dhabi. As these bioclasts are

349   transported and are, thus, not *in situ*, they can not be directly employed in the palaeoenvironmental

350   analysis of the depositional environment of the skeleton. However, the diverse assemblage, as

351 documented by Stewart et al. (2011) is consistent with the range of environments, from hypersaline

352 intertidal to less-saline shallow subtidal settings associated with the Recent coastline of Abu Dhabi.

353 The thin sub-vertical burrows observed in the subtidal sequence have previously been interpreted as

354 rootlets produced by seagrass and, as such, have been posited as evidence of a lagoonal

355 environment (Strohmenger et al., 2010). These features are, in fact, the mm-diameter, mucus-lined

356 burrows of an arthropod of the class arachnida. This mite produces identical burrows in the

357 supratidal zone of the Recent Abu Dhabi sabkha. As these burrows cross-cut stratigraphy they are

358 not strictly diagnostic of the facies in which they occur.

359 A siliciclastic component is relatively common within the Recent sediments of the Abu Dhabi

360 shoreline. This material is primarily derived from subaerially-exposed erosional remnants of the

361 middle-late Pleistocene Ghayathi Formation in the supratidal zone and generally reduces in

362 abundance distally into the lower intertidal to subtidal zone (Lokier et al., 2013). The lack of

363 siliciclastic material in the units associated with, and immediately overlying, the skeleton (Fig. 5) is

364 consistent with deposition in a setting at some distance from the supratidal zone.

365 The laterally-continuous iron oxide-stained horizons (Fig. 2) have previously been interpreted as

366 marking the positions of a fluctuating groundwater table (Kirkham, 1998).

367 The skeleton's location in relation to the present day coastline infers a minimum progradation of the

368 coast of 8.3 km since the whale was deposited, this equates to a progradation rate of between 1.56-

369 1.81 m/yr. This progradation rate lies within the range of 1.5-2 m/yr proposed from previous studies

370 of the sabkha system (Kenig, 1991; Kinsman and Park, 1976; Patterson and Kinsman, 1977; Warren,

371 2006) but is significantly higher than an average rate of 0.75 m/yr as previously proposed for the

372 more recent, post 1.4 ka, seaward portion of the sabkha system (Lokier and Steuber, 2008). This

373 disparity is consistent with the slowing of progradation rates over time, implying rates exceeding

374   1.81 m/yr prior to 1.4 ka. A rapid fall in sea level resulted in forced regression that was followed by

375   normal progradation as sea levels stabilised at a lower level (Fig. 6).

376

377   *Implications for mid- to late Holocene relative sea level*

378   The sedimentary sequence observed at the Mussafah Channel is interpreted in the context of a

379   whale beaching event as a complete parasequence recording a single flooding episode followed by a

380   relative sea level fall. As mentioned previously, the microbial mat belt in the Recent Abu Dhabi

381   sabkha is constrained to the landward limit of the intertidal zone, and is therefore effectively a

382   datum recording the height of mean higher high water (MHHW). We can assume that the buried,

383   ancient, microbial mat observed in the Mussafah Channel stratigraphic section was developed in a

384   similar environment and, thus, records MHHW at the time of microbial mat growth. Today, the

385   height of MHHW for the Umm Al Nar tide gauge (Fig. 1) is 1.64 m (Mohamed, 2008). The ancient

386   microbial mat at the Mussafah Channel section lies at 1.85 m above chart datum, it can therefore be

387   inferred that sea levels were 20 cm higher than today at 7103-6887 cal yr BP (Fig. 6). The effect of

388   post-depositional compaction on a sedimentary section of approximately 1 m thickness would be

389   negligible (Brain et al., 2012), however, it remains possible that the actual sea level was slightly in

390   excess of 20 cm.

391   The succession of the microbial mat by a hardground horizon records a retrogradational geometry

392   during continued flooding from 6887-6567 cal yr BP, with an additional 1.1 m of carbonate and

393   evaporite sediments being deposited above the microbial mat (Fig. 2). In peritidal carbonate settings

394   it has been inferred that accommodation space will be completely infilled by sediments (Fischer,

395   1964) however recent research has called this traditional 'accommodation filling' view into doubt

396   (Boss and Rasmussen, 1995; Eberli, 2013; Wilkinson et al., 1997). It is now recognised that

397   accommodation space is filled irregularly, this is due to the off-bank transport of carbonate material

398   by tides, wave currents and storms (Eberli, 2013). Given these factors, along with the unknown

399   degree of compaction, it is unlikely that the 1.3 m of section that lies above current MHHW

400   accurately records the true amplitude of the late Holocene sea level highstand. Instead, this figure

401   should be considered as a minimum value for the highstand (Fig. 6).

402   A further complicating factor in estimating the amplitude of the late Holocene highstand is the

403   displacive growth of evaporite minerals in the sedimentary column. In the Mussafah Channel setting,

404   between 26 to 34 cm thickness of evaporite-dominated sediments are recorded (Figs 2 & 5). These

405   units have developed through displacive interstitial growth in the supratidal setting and have

406   therefore increased the thickness of the sediment pile by approximately 30 cm. A final complicating

407   factor in estimating the late Holocene highstand is that, following sea level fall, after 5285-4574 cal

408   yr BP, it is likely that the sediment pile was deflated to within 50 cm of the groundwater table, as is

409   observed in the Abu Dhabi sabkha today.

410   Previous dates for the timing of the late Holocene highstand at the Abu Dhabi shoreline have varied

411   widely. The transgressive phase has been dated as exceeding current sea levels at between 7000 -

412   6000 BP (Evans et al., 1969; Lambeck, 1996) and reaching a maximum of 1-2 m above current sea

413   level (Evans et al., 1973; Kenig, 1991; Lambeck, 1996; Uchupi et al., 1996; Williams and Walkden,

414   2002) by between 6000-3400 BP (Evans et al., 1973; Evans et al., 1969; Kenig, 1991; Uchupi et al.,

415   1996; Williams and Walkden, 2002). Sea level fall has been dated as commencing between 4500-

416   2300 BP (Evans et al., 1969; Uchupi et al., 1996; Williams and Walkden, 2002) and reached current

417   levels by 1600-1000 BP (Kenig, 1991; Uchupi et al., 1996). The large discrepancies between these

418   dates may be attributed to the wide variety of material selected for radiocarbon dating. Many of the

419   studies employed bulk sediment samples or the shells of detrital feeding organisms as the source of

420   carbon, both of which are inherently unreliable for dating. A further source of error is that none of

421   these studies undertook a calibration of the radiocarbon ages in order to take account of the marine

422   reservoir effect.

423   An additional complication to the Quaternary history of the Persian Gulf has recently been

424   introduced by Wood et al. (2012) who have proposed a tectonic uplift of 125 m over the last 18 ka,

425   with current uplift rates of 1 mm/yr. Given that the relief of the Mussafah Channel microbial mat is

426   akin to present day MHHW, such a rate of tectonic uplift would necessitate a eustatic sea level rise

427   of 7 m over the past 7,000 years with a stillstand in the shoreline of the Persian Gulf over this period

428   – a hypothesis that clearly is not supported by any observational evidence, both in this study and

429   elsewhere. Thus, our observations support the hypothesis that the southern shore of the Persian

430   Gulf has been tectonically stable throughout the late Quaternary (Stevens et al., 2014).

431   In conclusion, the mid- to late Holocene sea level highstand surpassed present day sea level at 7100-

432   6890 cal yr BP and reached a minimum amplitude of 1 m above current sea level (Fig. 6).

433   Unfortunately, due to a lag in sediment deposition and the effects of deflation, it is not possible to

434   constrain the upper limit or the exact timing of this sea level peak other than stating that this must

435   have occurred after 5290-4570 cal yr BP. On the basis of previous observations of the progradational

436   sabkha sequence (Lokier and Steuber, 2008) it is inferred that sea level had fallen to near current

437   levels by 1440-1170 cal yr BP.

438

439   *Regional and global context*

440   The new results from the United Arab Emirates place accurate constraints as to the timing of the

441   transgressive, highstand and regressive episodes associated with the mid- to late Holocene sea level

442   high, both in the context of the Persian Gulf and at a broader, global, perspective. Although the

443   timing and elevation of the Holocene highstand has been reported as varying both spatially and

444   temporally (Murray-Wallace, 2007) these new results are comparable to those observed elsewhere

445   throughout the Indian Ocean region (Table 5) (Horton et al., 2005; Kench et al., 2009; Ramsay, 1996;

446   Ranasinghe et al., 2013; Woodroffe and Horton, 2005). Small disparities in the timing (on the scale of

447   a few hundreds of years) and amplitude (by up to +2 m) of the highstand between these areas are

448   inferred to result from hydro-isostatic effects and mantle rheology (Milne et al., 2009; Stattegger et

449   al., 2013; Woodroffe and Horton, 2005).

450   These new limits as to the timing of the mid- to late Holocene sea level highstand in the Persian Gulf

451   also compares favourably with previously proposed, though, often, less well-constrained, dates for

452   the transgressive and regressive phases from SE Asia (Chappell and Polach, 1991; Geyh et al., 1979;

453   Scoffin and Le Tissier, 1998; Stattegger et al., 2013; Tjia, 1996; Woodroffe and McLean, 1990; Yim

454   and Huang, 2002), Australia (Baker and Haworth, 2000; Baker et al., 2001; Beaman et al., 1994;

455   Collins et al., 2006; Flood and Frankel, 1989), the Pacific (Grossman et al., 1998; Nunn and Peltier,

456   2001) and the Atlantic (Angulo et al., 2006; Bourrouilh-Le Jan, 2007; Compton, 2001; Gayes et al.,

457   1992; van Soelen et al., 2010) regions (Table 5).

458   Many of these previous studies have been unable to decouple proposed eustatic sea level changes

459   from the signature of local and far field tectonic adjustments (Milne et al., 2009). The tectonically

460   stable southern shoreline of the Persian Gulf (Stevens et al., 2014) has not been affected either by

461   glacio-isostatic adjustment or by the far field effects of isostatic loading. We are therefore able to

462   confidentially establish that the mid- to late Holocene sea level history of the Persian Gulf is driven

463   by eustatic sea level without any influence from regional tectonic events.

464

465   **Conclusions**

466   The data from this study refine our knowledge of the timing of the transgression and regression

467   phases associated with the global mid- to late Holocene sea level highstand. We establish that mid-

468   Holocene transgression exceeded present day sea level by 7100-6890 cal yr BP with a highstand of >

469   1 m above current seal level being reached shortly after 5290-4570 cal yr BP. Subsequent relative

470   sea level fall had attained current datum by 1440-1170 cal yr BP. These new dates allow us to hone

471   previously-defined dates for the mid- to late Holocene sea level highstand from other regions,

472   thereby constraining the timing of this correlatable global eustatic event.

473   The Mussafah Channel cetacean was emplaced during the mid-Holocene transgressive phase, being

474   beached between 5300-4960 cal yr BP into an intertidal hardground pond. Paleoenvironmental

475   regimes in this setting, in terms of temperature, salinity and energy, are inferred to have been akin

476   to those observed at the coastline of Abu Dhabi today. Continued transgression saw the burial of the

477   skeleton within shallow-subtidal sediments before the relative sea level fall resulted in a forced

478   regression and a consequent rapid progradation in facies. We infer that the southern shoreline of

479   the Persian Gulf was tectonically stable at this time with relative sea level being driven by global

480   eustasy.

481   This study also illustrates the potential pitfalls of applying optically stimulated luminescence dating

482   techniques in isolation within sabkha environments. In arid coastal environments a high evaporation

483   rate in association with fluctuating saline groundwater levels may result in leaching and

484   concentration of uranium and potassium with consequent post-burial modifications of the

485   environmental radiation dose. Thus, measured elemental concentrations may not reflect the

486   average concentrations during the burial history of the sediments. This finding has important

487   implications for studies in similar settings where optically stimulated luminescence may be

488   employed as the sole dating method.

489

493   astute comments and suggestions that, we believe, have enhanced the quality of this manuscript. SL

494   also thanks Ali AL-Kaabi for assistance in the field and making his samples available for analysis.

495

496   **References**

497   Angulo, R.J., Lessa, G.C., Souza, M.C.d., 2006. A critical review of mid- to late-Holocene sea-level

498   fluctuations on the eastern Brazilian coastline. Quaternary Science Reviews 25, 486-506.

499   Baker, R.G.V., Haworth, R.J., 2000. Smooth or oscillating late Holocene sea-level curve? Evidence

500   from the palaeo-zoology of fixed biological indicators in east Australia and beyond. Marine Geology

501   163, 367-386.

502   Baker, R.G.V., Haworth, R.J., Flood, P.G., 2001. Inter-tidal fixed indicators of former Holocene sea

503   levels in Australia: a summary of sites and a review of methods and models. Quaternary

504   International 83–85, 257-273.

505   Banerjee, D., Murray, A.S., Bøtter-Jensen, L., Lang, A., 2001. Equivalent dose estimation using a

506   single aliquot of polymineral fine grains. Radiation Measurements 33, 73-94.

507   Bateman, M.D., Boulter, C.H., Carr, A.S., Frederick, C.D., Peter, D., Wilder, M., 2007. Detecting post-

508   depositional sediment disturbance in sandy deposits using optical luminescence. Quaternary

509   Geochronology 2, 57-64.

510   Beaman, R., Larcombe, P., Carter, R.M., 1994. New evidence for the Holocene sea-level high from

511   the inner shelf, central Great Barrier Reef, Australia. Journal of Sedimentary Research 64, 881-885.

512   Bosch, D.T., Dance, S.P., Moolenbeek, R.G., Oliver, P.G., 1995. Seashells of Eastern Arabia. Motivate

513   Publishing, Dubai.

514   Boss, S.K., Rasmussen, K.A., 1995. Misuse of Fischer plots as sea-level curves. Geology 23, 221-224.

515   Bottomley, N., 1996. Recent climate of Abu Dhabi, in: Osborne, P.E. (Ed.), Desert ecology of Abu

516   Dhabi. A review and recent studies. Pisces, Newbury, pp. 36-49.

517   Bourrouilh-Le Jan, F.G., 2007. Very high energy sedimentation (supratidal hurricane deposits) and

518   Mid-Holocene highstand on carbonate platforms, Andros, Bahamas: An alternative view.

519   Sedimentary Geology 199, 29-49.

520   Brain, M.J., Long, A.J., Woodroffe, S.A., Petley, D.N., Milledge, D.G., Parnell, A.C., 2012. Modelling

521   the effects of sediment compaction on salt marsh reconstructions of recent sea-level rise. Earth and

522   Planetary Science Letters 345-348, 180-193.

523   Cazenave, A., Nerem, R.S., 2004. Present-day sea level change: Observations and causes. Rev.

524   Geophys. 42, RG3001.

525   Chappell, J., Polach, H., 1991. Post-glacial sea-level rise from a coral record at Huon Peninsula, Papua

526   New Guinea. Nature 349, 147-149.

527   Clark, P.U., Dyke, A.S., Shakun, J.D., Carlson, A.E., Clark, J., Wohlfarth, B., Mitrovica, J.X., Hostetler,

528   S.W., McCabe, A.M., 2009. The Last Glacial Maximum. Science 325, 710-714.

529   Collins, L.B., Zhao, J.-X., Freeman, H., 2006. A high-precision record of mid–late Holocene sea-level

530   events from emergent coral pavements in the Houtman Abrolhos Islands, southwest Australia.

531   Quaternary International 145–146, 78-85.

532   Compton, J.S., 2001. Holocene sea-level fluctuations inferred from the evolution of depositional

533   environments of the southern Langebaan Lagoon salt marsh, South Africa. The Holocene 11, 395-

534   405.

535   Eberli, G.P., 2013. The uncertainties involved in extracting amplitude and frequency of orbitally

536   driven sea-level fluctuations from shallow-water carbonate cycles. Sedimentology 60, 64-84.

537   Evans, G., Murray, J.W., Biggs, H.E.J., Bate, R., Bush, P.R., 1973. The oceanography, ecology,

538   sedimentology and geomorphology of parts of the Trucial Coast barrier island complex, Persian Gulf,

539   in: Purser, B.H. (Ed.), The Persian Gulf - Holocene Carbonate Sedimentation and Diagenesis in a

540   Shallow Epicontinental Sea. Springer-Verlag, Berlin, pp. 233-277.

541   Evans, G., Schmidt, V., Bush, P., Nelson, H., 1969. Stratigraphy and geologic history of the sabkha,

542   Abu Dhabi, Persian Gulf. Sedimentology 12, 145-159.

543   Fischer, A.G., 1964. The Lofer Cyclothems of the Alpine Triassic. Kansas Geological Survey, Bulletin

544   169, 107-149.

545   Fleming, K., Johnston, P., Zwartz, D., Yokoyama, Y., Lambeck, K., Chappell, J., 1998. Refining the

546   eustatic sea-level curve since the Last Glacial Maximum using far- and intermediate-field sites. Earth

547   and Planetary Science Letters 163, 327-342.

548   Flood, P.G., Frankel, E., 1989. Late Holocene higher sea level indicators from eastern Australia.

549   Marine Geology 90, 193-195.

550   Galbraith, R.F., Green, P.F., 1990. Estimating the component ages in a finite mixture. International

551   Journal of Radiation Applications and Instrumentation. Part D. Nuclear Tracks and Radiation

552   Measurements 17, 197-206.

553   Gayes, P.T., Scott, D.B., Collins, E.S., Nelson, D.D., 1992. A Late Holocene sea-level fluctuation in

554   South Carolina, in: Fletcher III, C.H., Wehmiller, J.F. (Eds.), Quaternary coasts of the United States:

555   Marine and Lacustrine Systems. SEPM, pp. 155-160.

556   Geyh, M.A., Streif, H., Kudrass, H.R., 1979. Sea-level changes during the late Pleistocene and

557   Holocene in the Strait of Malacca. Nature 278, 441-443.

558   Goodwin, D.H., Schone, B.R., Dettman, D.L., 2003. Resolution and Fidelity of Oxygen Isotopes as

559   Paleotemperature Proxies in Bivalve Mollusk Shells: Models and Observations. PALAIOS 18, 110-125.

560   Grossman, E.E., Fletcher Iii, C.H., Richmond, B.M., 1998. The Holocene sea-level highstand in the

561   equatorial Pacific: analysis of the insular paleosea-level database. Coral Reefs 17, 309-327.

562   Hanebuth, T.J.J., Stattegger, K., Bojanowski, A., 2009. Termination of the Last Glacial Maximum sea-

563   level lowstand: The Sunda-Shelf data revisited. Global and Planetary Change 66, 76-84.

564   Horton, B.P., Gibbard, P.L., Mine, G.M., Morley, R.J., Purintavaragul, C., Stargardt, J.M., 2005.

565   Holocene sea levels and palaeoenvironments, Malay-Thai Peninsula, southeast Asia. The Holocene

566   15, 1199-1213.

567   Hughen, K.A., Baillie, M.G.L., Bard, E., Bayliss, A., Beck, J.W., Bertrand, C.J.H., Blackwell, P.G., Buck,

568   C.E., Burr, G.S., Cutler, K.B., Damon, P.E., Edwards, R.L., Fairbanks, R.G., Friedrich, M., Guilderson,

T.P., Kromer, B., McCormac, F.G., Manning, S.W., Bronk Ramsey, C., Reimer, P.J., Reimer, R.W.,

Remmele, S., Southon, J.R., Stuiver, M., Talamo, S., Taylor, F.W., van der Plicht, J., Weyhenmeyer,

C.E., 2004. Marine04 Marine radiocarbon age calibration, 26 - 0 ka BP. Radiocarbon 46, 1059-1086.

Kench, P.S., Smithers, S.G., McLean, R.F., Nichol, S.L., 2009. Holocene reef growth in the Maldives:

Evidence of a mid-Holocene sea-level highstand in the central Indian Ocean. Geology 37, 455-458.

Kenig, F., 1991. Sédimentation, distribution et diagenèse de la matière organique dans un

environment carbonaté hypersalin: le système lagune-sabkha d'Abu Dhabi, Institut Français du

Pétrole. Université d'Orléans, France, p. 328.

Kenig, F., Huc, A.Y., Purser, B.H., Oudin, J.L., 1990. Sedimentation, distribution and diagenesis of

organic-matter in a recent carbonate environment, Abu-Dhabi, UAE. Organic Geochemistry 16, 735-

747.

Kinsman, D.J.J., 1964. Reef coral tolerance of high temperature and salinites. Nature, 1280-1282.

Kinsman, D.J.J., Park, R.K., 1976. Algal belt and coastal sabkha evolution, Trucial Coast, Persian Gulf,

in: Walter, M.H. (Ed.), Stromatolites. Elsevier, pp. 421-433.

Kirkham, A., 1998. A Quaternary proximal foreland ramp and its continental fringe, Arabian Gulf,

UAE, in: Wright, V.P., Burchette, T.P. (Eds.), Carbonate Ramps. Geological Society, London, pp. 15-41.

Lambeck, K., 1996. Shoreline reconstructions for the Persian Gulf since the last glacial maximum.

Earth and Planetary Science Letters 142, 43-57.

Leuliette, E., Nerem, R., Mitchum, G., 2004. Calibration of TOPEX/Poseidon and Jason Altimeter Data

to Construct a Continuous Record of Mean Sea Level Change. Marine Geodesy 27, 79-94.

Lian, O.B., Hu, J., Huntley, D.J., Hicock, S.R., 1995. Optical dating studies of Quaternary organic-rich

sediments from southwestern British Columbia and northwestern Washington State. Canadian

Journal of Earth Sciences 32, 1194-1207.

Lokier, S., Steuber, T., 2008. Quantification of carbonate-ramp sedimentation and progradation rates

for the late Holocene Abu Dhabi shoreline. Journal of Sedimentary Research 78, 423-431.

594   Lokier, S., Steuber, T., 2009. Large-scale intertidal polygonal features of the Abu Dhabi coastline.

595   Sedimentology 56, 609-621.

596   Lokier, S.W., 2012. Development and evolution of subaerial halite crust morphologies in a coastal

597   sabkha setting. Journal of Arid Environments 79, 32-47.

598   Lokier, S.W., Knaf, A., Kimiagar, S., 2013. A quantitative analysis of Recent arid coastal sedimentary

599   facies from the Arabian Gulf Coastline of Abu Dhabi, United Arab Emirates. Marine Geology 346,

600   141-152.

601   Milne, G.A., Gehrels, W.R., Hughes, C.W., Tamisiea, M.E., 2009. Identifying the causes of sea-level

602   change. Nature Geosci 2, 471-478.

603   Mohamed, K.A., 2008. Long-term tidal water level measurements in Abu Dhabi Emirate, ASME 27th

604   International Conference on Offshore Mechanics and Arctic Engineering. ASME, Estoril, Portugal, pp.

605   937-944.

606   Murray-Wallace, C.V., 2007. Eustatic sea-level chnages since the last glaciation, in: Ellias, S.A. (Ed.),

607   Encyclopedia of Quaternary Science. Elsevier, Amsterdam, pp. 3034-3043.

608   Murray, A.S., Wintle, A.G., 2000. Luminescence dating of quartz using an improved single-aliquot

609   regenerative-dose protocol. Radiation Measurements 32, 57-73.

610   Nunn, P.D., Peltier, W.R., 2001. Far-Field Test of the ICE-4G Model of Global Isostatic Response to

611   Deglaciation Using Empirical and Theoretical Holocene Sea-Level Reconstructions for the Fiji Islands,

612   Southwestern Pacific. Quaternary Research 55, 203-214.

613   Patterson, R.J., Kinsman, D.J.J., 1977. Marine and continental groundwater sources in a Persian Gulf

614   coastal sabkha, Reefs and Related Carbonates - Ecology and Sedimentology. AAPG, pp. 381-397.

615   Peltier, W.R., Fairbanks, R.G., 2006. Global glacial ice volume and Last Glacial Maximum duration

616   from an extended Barbados sea level record. Quaternary Science Reviews 25, 3322-3337.

617   Prescott, J.R., Hutton, J.T., 1994. Cosmic ray contributions to dose rates for luminescence and ESR

618   dating: Large depths and long-term time variations. Radiation Measurements 23, 497-500.

619   Purser, B.H., Evans, G., 1973. Regional sedimentation along the Trucial Coast, SE Persian Gulf, in:

620   Purser, B.H. (Ed.), The Persian Gulf - Holocene Carbonate Sedimentation and Diagenesis in a Shallow

621   Epicontinental Sea. Springer-Verlag, Berlin, pp. 211-231.

622   Raafat, H., 2007. Climate, in: Kumar, A. (Ed.), Physical Geography Sector Paper. Environment Agency

623   Abu Dhabi, pp. 72-89.

624   Ramsay, P.J., 1996. 9000 Years of sea-level change along the southern African coastline. Quaternary

625   International 31, 71-75.

626   Ranasinghe, P.N., Ortiz, J.D., Moore, A.L., McAdoo, B., Wells, N., Siriwardana, C.H.E.R., Wijesundara,

627   D.T.D.S., 2013. Mid–Late Holocene coastal environmental changes in southeastern Sri Lanka: New

628   evidence for sea level variations in southern Bay of Bengal. Quaternary International 298, 20-36.

629   Sarnthein, M., 1972. Sediments and history of the Postglacial transgression in the Persian Gulf and

630   northwest Gulf of Oman. Marine Geology 12, 245-266.

631   Scoffin, T.P., Le Tissier, M.D.A., 1998. Late Holocene sea level and reef flat progradation, Phuket,

632   South Thailand. Coral Reefs 17, 273-276.

633   Shinn, E.A., 1969. Submarine lithification of Holocene carbonate sediments in the Persian Gulf.

634   Sedimentology 12, 109-144.

635   Stattegger, K., Tjallingii, R., Saito, Y., Michelli, M., Trung Thanh, N., Wetzel, A., 2013. Mid to late

636   Holocene sea-level reconstruction of Southeast Vietnam using beachrock and beach-ridge deposits.

637   Global and Planetary Change 110, Part B, 214-222.

638   Stevens, T., Jestico, M.J., Evans, G., Kirkham, A., 2014. Eustatic control of late Quaternary sea-level

639   change in the Arabian/Persian Gulf. Quaternary Research 82, 175-184.

640   Stewart, J.R., Aspinall, S., Beech, M., Fenberg, P., Hellyer, P., Larkin, N., Lokier, S.W., Marx, F.G.,

641   Meyer, M., Miller, R., Rainbow, P.S., Taylor, J.D., Whittaker, J.E., Al-Mehsin, K., Strohmenger, C.J.,

642   2011. Biotically constrained palaeoenvironmental conditions of a mid-Holocene intertidal lagoon on

643   the southern shore of the Arabian Gulf: evidence associated with a whale skeleton at Musaffah, Abu

644   Dhabi, UAE. Quaternary Science Reviews 30, 3675-3690.

645   Strohmenger, C.J., Al-Mansoori, A., Al-Jeelani, O., Al-Shamry, A., Al-Hosani, I., Al-Mehsin, K., Shebl,

646   H., 2010. The sabkha sequence at Mussafah Channel (Abu Dhabi, United Arab Emirates): Facies

647   stacking patterns, microbial-mediated dolomite and evaporite overprint. GeoArabia 15, 49-90.

648   Stuiver, M., Polach, H.A., 1977. Discussion reporting of 14C data. Radiocarbon 19, 355-363.

649   Stuiver, M., Reimer, P.J., 1993. Extended 14C database and revised CALIB radiocarbon calibration

650   program. Radiocarbon 35.

651   Taylor, S.R., McClennan, S.M., 1985. The continental crust: Its composition and evolution. Blackwell

652   Scientific Publications, Oxford.

653   Tjia, H.D., 1996. Sea-level changes in the tectonically stable Malay-Thai Peninsula. Quaternary

654   International 31, 95-101.

655   Uchupi, E., Swift, S.A., Ross, D.A., 1996. Gas venting and late Quaternary sedimentation in the

656   Persian (Arabian) Gulf. Marine Geology 129, 237-269.

657   van Soelen, E.E., Lammertsma, E.I., Cremer, H., Donders, T.H., Sangiorgi, F., Brooks, G.R., Larson,

658   R.A., Sinninghe Damsté, J.S., Wagner-Cremer, F., Reichart, G.J., 2010. Late Holocene sea-level rise in

659   Tampa Bay: Integrated reconstruction using biomarkers, pollen, organic-walled dinoflagellate cysts,

660   and diatoms. Estuarine, Coastal and Shelf Science 86, 216-224.

661   Walker, M., 2005. Quaternary Dating Methods. John Wiley & Sons, Ltd.

662   Warren, J.K., 2006. Evaporites: Sediments, Resources and Hydrocarbons. Pringer.

663   Wilkinson, B.H., Drummond, C.N., Rothman, E.D., Diedrich, N.W., 1997. Stratal order in peritidal

664   carbonate sequences. Jounrnal of Sedimentary Research 67, 1068-1082.

665   Williams, A.H., Walkden, G.M., 2002. Late Quaternary highstand deposits of the southern Arabian

666   Gulf: a record of sea-level and climate change, in: Clift, P.D., Kroon, D., Gaedicke, C. & Craig, J. (Ed.),

667   The Tectonic and Climatic Evolution of the Arabian Sea Region. Geological Society of London,

668   London, pp. 371-386.

669   Wilson, P., Vincent, P.J., Telfer, M.W., Lord, T.C., 2008. Optically stimulated luminescence (OSL)

670   dating of loessic sediments and cemented scree in northwest England. The Holocene 18, 1101-1112.

671   Wood, W.W., Bailey, R.M., Hampton, B.A., Kraemer, T.F., Lu, Z., Clark, D.W., James, R.H.R., Al

672   Ramadan, K., 2012. Rapid late Pleistocene/Holocene uplift and coastal evolution of the southern

673   Arabian (Persian) Gulf. Quaternary Research 77, 215-220.

674   Woodroffe, C., McLean, R., 1990. Microatolls and recent sea level change on coral atolls. Nature 344,

675   531-534.

676   Woodroffe, S.A., Horton, B.P., 2005. Holocene sea-level changes in the Indo-Pacific. Journal of Asian

677   Earth Sciences 25, 29-43.

678   Yim, W.W.S., Huang, G., 2002. Middle Holocene higher sea-level indicators from the south China

679   coast. Marine Geology 182, 225-230.

680   Yokoyama, Y., Lambeck, K., De Deckker, P., Johnston, P., Fifield, L.K., 2000. Timing of the Last Glacial

681   Maximum from observed sea-level minima. Nature 406, 713-716.

682

683

List of Tables

List of Figures

705   enterolithic anhydrite (e) and the prominent iron stained horizon (Fe). Note the large bone covered in plaster

706   of Paris (b) in the lower left corner of the section. Image A courtesy Nigel Larkin.

707   **5** The relationship between sedimentary facies and component allochems for the three logged sections.

708   **6** Relative sea level trends and relationships to the depositional facies observed within the Mussafah Channel

709   sequence.

Table 1

Section	Depth (cm)	Peloid	Ooid	Mud	Gypsum grain	Anhydrite	Quartz	Feldspar	Lithic grain	Calcite cement	Gypsum cement	Foraminifera	Bivalve	Gastropod	Echinoid	Ostracod	Bryozoan	Unidentified bioclast
	7	3.0				95.5										1.0		0.5
	19	23.0		62.0		13.5												1.5
	34	43.5		37.0	3.0							1.5				2.0		13.0
	53			84.0	6.0							1.5				1.0		7.5
MC1	65	12.0		85.0	2.0											0.5		0.5
	95	51.4		32.9	1.3									12.7				1.7
	105	27.3	0.3	17.7	1.8		1.8			15.5		2.4	1.8	21.6		0.3		9.5
	113	16.5		67.5	4.5		1.5		2.0									8.0
	131	33.2		26.9	9.0		1.0	1.0	3.0			2.0		0.5				23.4
	7	34.0		17.0	26.5	0.5	0.5					0.5			0.5		0.5	20.0
	24	37.5		47.5	10.0							2.0				0.5	1.0	1.5
MC2	35	54.2		37.8	1.5		0.5					1.5		0.5		0.5		3.5
	50	41.6		36.6	5.4	2.0						5.0	1.0			2.5		5.9
	80	43.2		42.7	7.8	1.0						1.9		2.9				0.5
	100	55.4	0.5	27.2	7.4	1.0			0.5			2.5		1.0				4.5
	10	5.0				94.0												1.0
	18	23.3		4.5	0.5	67.2						1.0		1.0				2.5
	27	23.6		66.4	2.5	0.5					3.0	0.5		1.5				2.0
	40	10.9		80.6	5.0							1.0		0.5				2.0
MC3	47	45.3		22.2	13.8						0.5	4.4		1.5		1.0		11.3
	58	0.5		90.5	5.5							3.0				0.5		
	70	58.2		32.8	4.0							2.0		0.5				2.5
	80	51.3		12.2	3.0						16.5	1.7	0.9	5.7		1.3		7.4
	88	52.0		31.5	12.0		0.5					1.0						3.0

Table 2

Sample Name	Laboratory Sample code	Nature of sample	Radiocarbon Age (^{14}C yr BP)	AMS δ^{13}C (‰)	Calibrated Age Range (2 σ) (cal yr BP)
MC02	UB16441	Bivalve shell from hardground	6452 ± 32	1	6887 - 6567
MUS 17B	UB16449	Bone	Undetermined		
MUS 28/01/08	UB16450	Barnacle *Coronula diadema* from close to left scapula	5032 ± 30	-4.7	5304 - 4957
MUS 09 110.M	UB16451	Articulated bivalve *Barbatia* from material next to vertebrae	4743 ± 27	-1.5	4914 - 4574
MUS 11	UB16452	*Barbatia* shell from orange shelly layer banked against skull	5002 ± 29	-0.8	5285 - 4922

Note: Calibration utilised the CALIB (version 7.0.0) (Stuvier and Reimer, 1993) to 2 sigma employing a marine calibration curve and a regional reservoir age correction (ΔR) of 180 ± 53 derived from a sample of known age collected within the Persian Gulf to the east of Qatar (Hughen et al., 2004).

Table 3

Sample	Laboratory code	Depth (cm)	Palaeodose (De) (Gy)	Dose rate (µGy/a-1)	OSL age (ka BP)
MUS OSL 1a	Shfd11039	137	4.05 ± 0.23	1275 ± 63	3.18 ± 0.24
MUS OSL 2a	Shfd11040	98	2.47 ±0.08	884 ± 46	2.79 ± 0.17
MUS OSL 3a	Shfd11041	68	2.40 ± 0.07	955 ± 47	2.51 ± 0.14
Adjusted for potential dose-rate problems (see text for details)					
MUS OSL 1a	Shfd11039	137	4.05 ± 0.23	675 ± 32	6.00 ± 0.45
MUS OSL 2a	Shfd11040	98	2.47 ±0.08	365 ± 14	6.76 ± 0.34
MUS OSL 3a	Shfd11041	68	2.40 ± 0.07	452 ± 18	5.31 ± 0.27

Note: Ages are presented at 1 sigma confidence incorporating systematic uncertainties with the dosimetry data, uncertainties with palaeomoisture and errors associated with De determination.
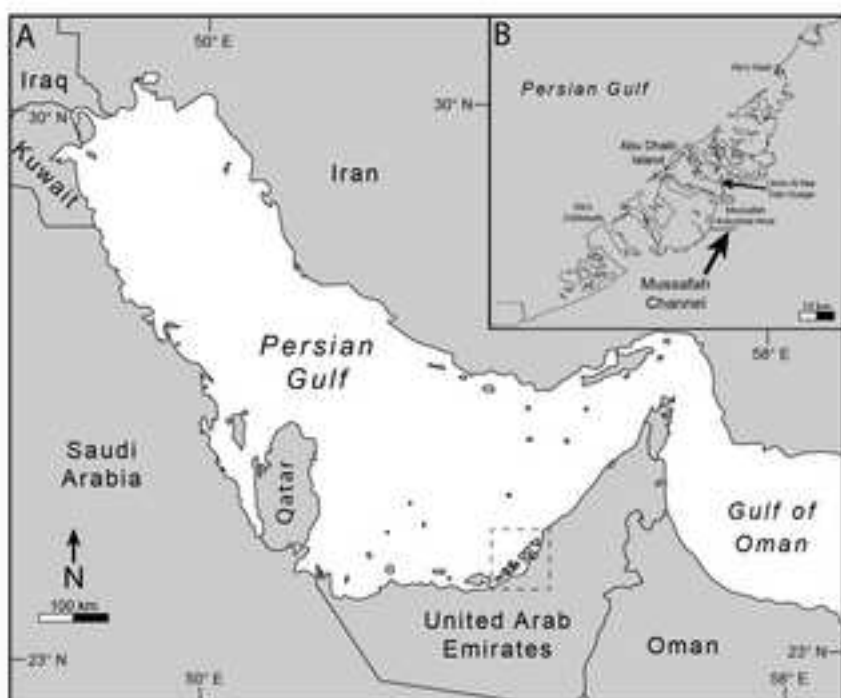
Table 4

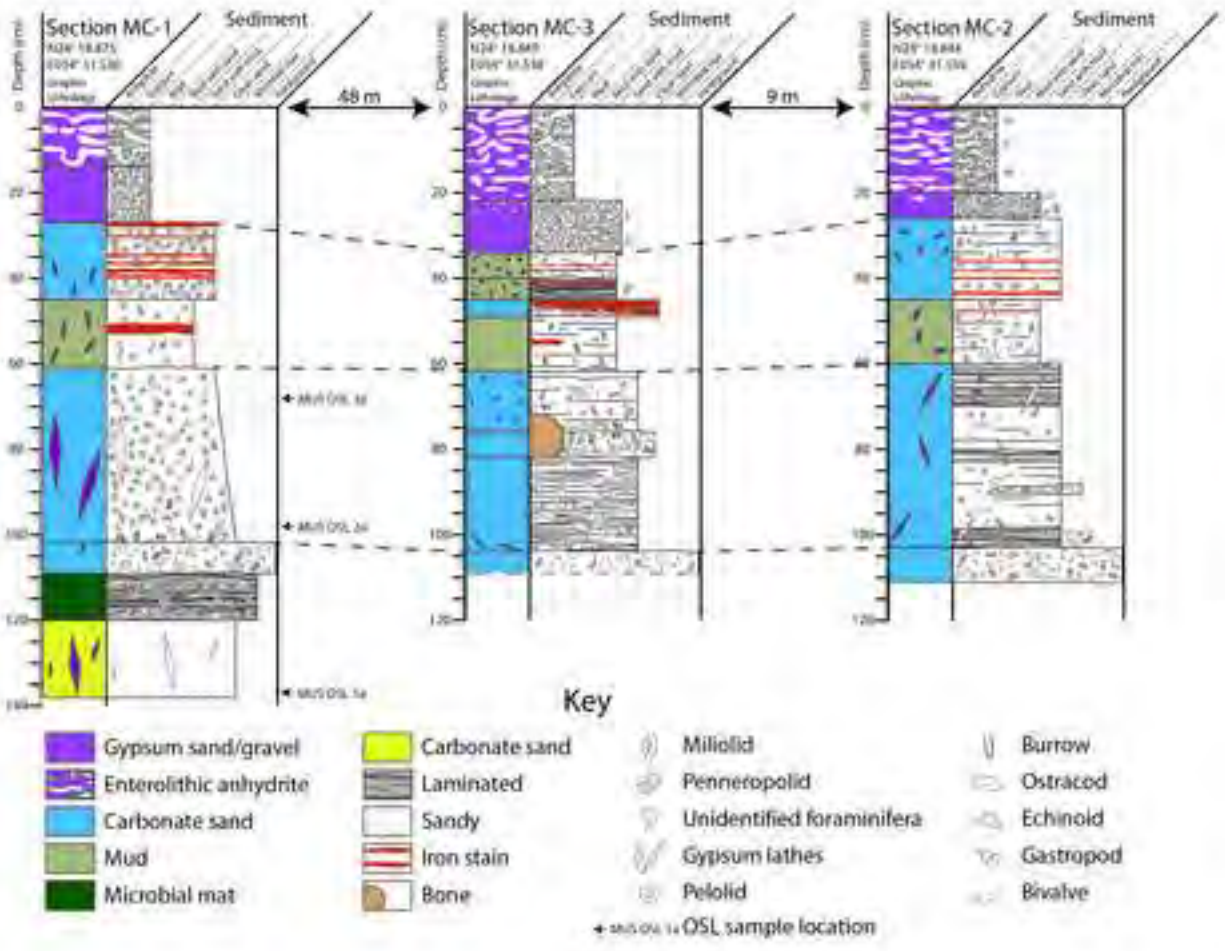| Sample name	Nature of sample	$\delta^{13}C$ (‰V-PDB)	$\delta^{18}O$ (‰V-PDB)	Calculated temperature (°C)
MUS09 110.M	Articulated bivalve *Barbatia* from next to whale	1.65	2.34	22.6
MUS09 148.M	Articulated bivalve *Pinctada* from next to whale	1.37	1.16	27.7
MUS09 183.M	Articulated bivalve *Pinctada* from next to whale	2.22	0.51	30.5

		$\delta^{13}C$ (‰V-PDB)	$\delta^{18}O$ (‰V-PDB)	Calculated temperature (°C)

Table 5

Location	Transgression past present sea level	Highstand	Regression to present sea level	Maximum sea level (+m)	Author
Indian Ocean					
Malay-Thai Peninsula		4850-4450 cal yr BP		5	Horton et al., 2005
Mozambique	6500 BP	4480 BP	900 BP	2.75	Ramsay, 1995
Maldives	4500 cal yr BP	4000-2100 cal yr BP		>0.5 ±1	Kench et al., 2009
Sri Lanka		4900-4000 BP	3000 BP		Ranasinghe et al., 2013
SE Asia					
Papua New Guinea		5800 ^{14}C yrs BP			Chappell and Polach, 1991
Strait of Malacca		4980 ^{14}C yrs BP		5	Geyh et al., 1979
Cocos Islands		after 3000 ^{14}C yrs BP		>0.5	Woodroffe and McLean, 1990
Phuket, Thailand		6000 BP		1	Scoffin and Le Tissier, 1998
S. China		5140 ±50 yr BP		<2	Yim and Huang, 2002
Thai-Malay Peninsula	6 ka	5 ka	1.5 ka (Thailand)	5	Tjia, 1996
Vietnam		6.7-5 ka		1.4-1.6	Stattegger et al., 2013
Australia					
W Australia		5660 ±50-4040 ±50 ^{14}C yrs BP		1.65	Beaman et al., 1994
E Australia		3420-1780 BP		>1	Flood and Frankel, 1989
E Australia		4150-3470 BP		1.7	Baker and Haworth, 2000
S Australia		5100 BP		2.2	Baker et al., 2000
SW Australia		7 ka		2	Collins et al., 2006
Pacific					
Central Equatorial Pacific		5000-1500 BP		1-2	Grossman et al., 1998
Fiji Islands	before 6900 ^{14}C yrs BP	5650-3200 ^{14}C yrs BP		1.35-1.5	Nunn and Peltier, 2001
Atlantic					
S Carolina, USA		4.2 ka			Gayes et al., 1992
Florida, USA	7.5 ka				Van Soelen et al., 2010
South Africa		6.8 ka	4.9 ka	0-3	Compton, 2001
Brazil	7550-6500 cal yr BP	5800-2000 cal yr BP		2-3	Angulo et al., 2006
Bahamas		3000 BP		1.5	Bourrouilh-Le Jan, 2007

Figure 1
Click here to download high resolution image

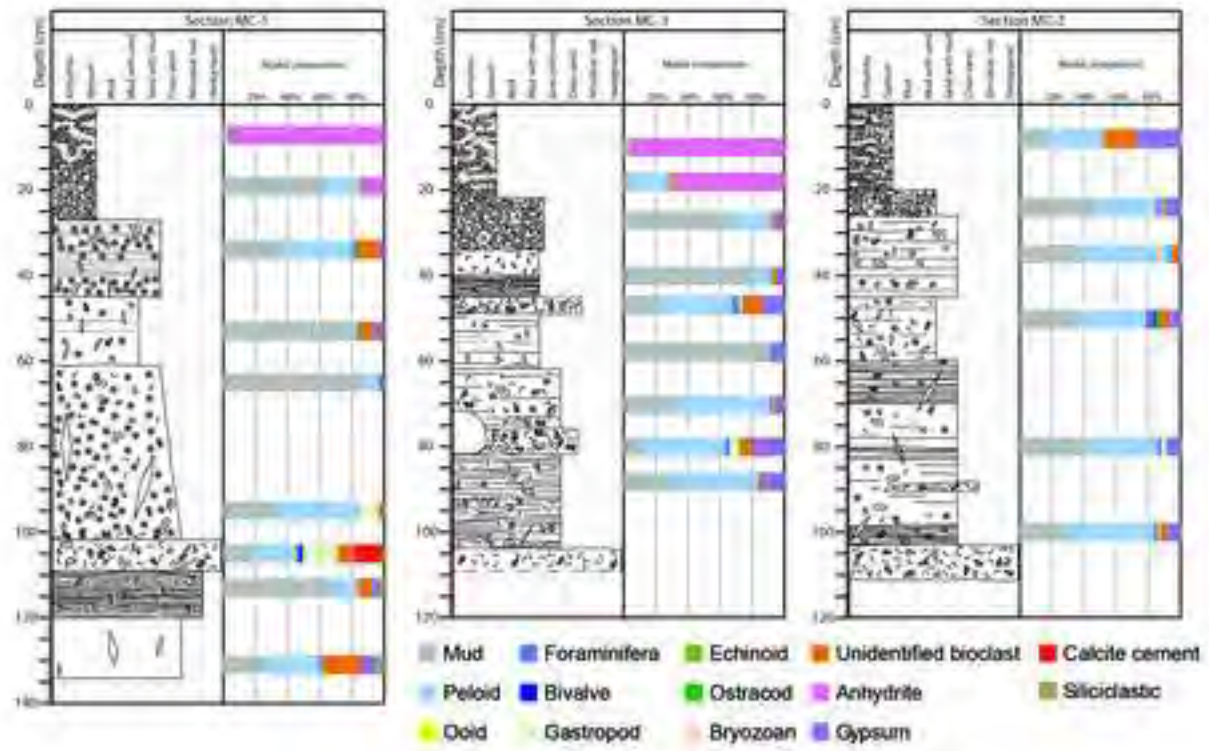**Figure 2**
Click here to download high resolution image

Key

Gypsum sand/gravel
Enterolithic anhydrite
Carbonate sand
Mud
Microbial mat

Carbonate sand
Laminated
Sandy
Iron stain
Bone

Miliolid
Penneropolid
Unidentified foraminifera
Gypsum lathes
Pelolid
OSL sample location

Burrow
Ostracod
Echinoid
Gastropod
Bivalve

Figure 3
Click here to download high resolution image

Figure 3

Figure 5
[Click here to download high resolution image](#)

Figure 5

Figure 6
Click here to download high resolution image